

Hysteresis curves reveal the microscopic origin of cooperative CO₂ adsorption in diamine-appended metal–organic frameworks

John R. Edison,^{1,2,*} Rebecca L. Siegelman,^{3,4,†} Zdeněk Preisler,^{1,†}
Joyjit Kundu,^{1,5,‡} Jeffrey R. Long,^{3,4,6,†} and Stephen Whitelam^{1,§}

¹*Molecular Foundry, Lawrence Berkeley National Laboratory, 1 Cyclotron Road, Berkeley, CA 94720, USA*

²*Martin A. Fisher School of Physics, Brandeis University, Waltham, MA 02454, USA*

³*Department of Chemistry, University of California, Berkeley, CA 94720, USA*

⁴*Materials Sciences Division, Lawrence Berkeley National Laboratory, Berkeley, CA 94720, USA*

⁵*Department of Chemistry, Duke University, Durham, NC 27708, USA*

⁶*Department of Chemical and Biomolecular Engineering,
University of California, Berkeley, CA 94720, USA*

Diamine-appended metal–organic frameworks (MOFs) of the form Mg₂(dobpdc)(diamine)₂ adsorb CO₂ in a cooperative fashion, exhibiting an abrupt change in CO₂ occupancy with pressure or temperature. This change is accompanied by hysteresis. While hysteresis is suggestive of a first-order phase transition, we show that hysteretic temperature-occupancy curves associated with this material are qualitatively unlike the curves seen in the presence of a phase transition; they are instead consistent with CO₂ chain polymerization, within one-dimensional channels in the MOF, in the absence of a phase transition. Our simulations of a microscopic model reproduce this dynamics, and point the way toward rational control, in and out of equilibrium, of cooperative adsorption in this industrially important class of materials.

Summary— Experiments and simulations of the dynamics of cooperative adsorption in diamine-appended MOFs reveal the underlying molecular mechanism.

Introduction— Metal–organic frameworks (MOFs) are porous, crystalline materials with large internal surface areas, and have been studied extensively as adsorbents for gas storage and separations [1–3]. The recently-developed MOFs Mg₂(dobpdc)(diamine)₂ are particularly promising in this regard because they exhibit cooperative adsorption, in which a conveniently small change in pressure or temperature results in an abrupt change in the quantity of CO₂ adsorbed by the framework [4–6]. In a majority of cases, cooperative adsorption results from a guest-induced phase transition or dynamic rearrangement of the MOF structure, or a phase transition in the diamine-appended MOFs proceeds through a one-dimensional chemical reaction. As described in Ref [5], proton transfer and nucleophilic attack of N on a CO₂ molecule forms an ammonium carbamate species that induces a chain reaction leading to the cooperative insertion of CO₂ into the metal-amine bonds to yield chains of ammonium carbamate along the pore axis. The one-dimensional nature of adsorption, and the physics of one-dimensional phenomena, suggests that cooperative gas uptake in diamine-appended Mg₂(dobpdc) materials occurs in the absence of a phase transition [14, 15]. Clarifying this issue is important in order to establish a microscopic understanding of cooperative gas uptake.

In this paper we study cooperative adsorption in the representative diamine-appended MOF e-2-Mg₂(dobpdc) (e-2 = *N*-ethylethylenediamine). We show that its *dynamics*, in the form of the hysteresis seen in temperature-occupancy curves, indicates that cooperative adsorption occurs in the absence of a phase transition. Hysteresis, a memory of the prior state of the system, is indeed normally associated with a first-order phase transition, which involves a discontinuous change of an order parameter (e.g. gas occupancy) with a control parameter (e.g. temperature). In this setting, hysteresis arises from the slow dynamics of nucleation, i.e. the potentially long time required for thermal fluctuations to produce a nucleus of the stable phase (during which time the system remains “stuck” in its initial state) [16, 17]. However, hysteresis results more generally whenever a system’s order parameter changes less rapidly than its control parameter, and so can also arise in the absence of a phase transition. For instance, force-extension curves for DNA stretching display hysteresis associated with the slow detachment of the two strands of the helix [18–21]. Here we present experimental and simulation data showing that the nature of hysteresis in temperature-occupancy data for CO₂ in e-2-Mg₂(dobpdc) is consistent with CO₂ polymerization in the absence of an underlying phase transition. Our work provides a link between microscopic models of gas adsorption and experimental data, and provides fundamental understanding of a phenomenon of experimental and industrial importance.

Hysteresis in gas-uptake data—To provide a basis for our claim we summarize in Fig. 1(a,c) the canonical case of hysteresis accompanying a first-order phase transition. In panel (a) we show typical adsorption-desorption curves [22] for an ordered porous material with a narrow pore-size distribution, as a function of temperature T , for the case in which the adsorbate or framework un-

* dayakaran@brandeis.edu; Corresponding author

† All authors contributed equally to this work

‡ joyjitkundu032@gmail.com; Corresponding author

§ swhitelam@lbl.gov; Corresponding author

dergoes a first-order phase transition (or a “rounded” transition if the system is of finite size [23]). In panel (c) we show the accompanying free-energy landscape for a single pore [16, 17].

The origin of hysteresis in this scenario is the slow dynamics of nucleation: we must wait for a thermal fluctuation to generate a nucleus of the stable phase. Near phase coexistence the nucleation time is large, and can therefore exceed the experimental observation time. However, the system retains the ability to relax to the local or metastable equilibrium as T is varied [24]. This separation of timescales can be identified by “early stop” desorption scans, initiated partway up the adsorption curve. One such example is shown as a black dashed line in panel (a). As T increases (moving left on the figure) the adsorbate loading (dashed line) decreases monotonically: pores that are empty when the desorption scan begins remain so as the scan proceeds [25–29] (see e.g. Fig. 17 of Ref. [17]). Materials that display adsorption hysteresis due to an underlying structural transition show similar behavior [30].

By contrast, we expect early-stop desorption experiments in the absence of a phase transition to behave as shown in Fig. 1(b). The associated free-energy surface, shown in panel (d), has a single minimum under all conditions, and the system should be able to evolve in the direction of this minimum on the timescale of the experiment. The result is a non-monotonic early-stop desorption curve.

Experimental data are consistent with the absence of a phase transition— In Fig. 2(a) we show experimental adsorption and desorption curves for CO₂ in the representative diamine-appended MOF e-2-Mg₂(dobpdc); see Appendix A for experimental details. In the figure we also show early-stop desorption curves (dotted lines) obtained by reversing the temperature scan partway up the adsorption curve. These curves indeed behave according to the scenario shown in panel (b) of Fig. 1: the dynamics of cooperative adsorption in this MOF are qualitatively consistent with loading that proceeds in the absence of a phase transition. Similar non-monotonic behavior has been predicted to occur when diffusion of the gas molecules within the framework is much slower than experimental timescales [31]. Estimates of diffusivities from NMR measurements [32] for our system rule out this scenario.

Modeling reveals the microscopic origin of hysteresis— In Fig. 2(b) we show analogous data obtained from dynamic simulations of the statistical mechanical model of Ref. [15]. This model captures the cooperative CO₂ adsorption behavior of the diamine-appended MOFs by modeling the polymerization of ammonium carbamate chains along the pore direction. Analysis of the model indicates that such polymerization results in a step-like isotherm in the absence of a phase transition. The model’s dynamical behavior, presented here, is consistent with the experimental data of Fig. 2(a), and with the mechanism summarized by Fig. 1(b). For computa-

tional efficiency we performed the simulations at a higher temperature range (540 – 750 K) than the experiments ($\approx 380 - 420$ K). The solid line marked “equilibrium” in Fig. 2(b) is obtained by transfer-matrix calculation, while the colored lines are obtained by dynamical simulation.

In more detail, the model, sketched in Fig. 3(a), is a representation of part of a one-dimensional channel of a diamine-appended MOF. The degrees of freedom of the model relate to the CO₂ binding states of the appended diamines, and we distinguish between CO₂ molecules bound singly or as part of a polymerized chain. The energetic parameters of the model are chosen to model Mg metal sites, and the dynamics of the model is propagated using a standard continuous-time Monte Carlo scheme [33]; details are given in Appendix B. Cooperative adsorption in this model results from an abrupt (but finite) growth in the mean length of polymerized CO₂ chains with temperature, and the resulting adsorption curves agree qualitatively and semi-quantitatively with experimental data [15]. Here we show that the accompanying dynamics is also consistent with experiment. Computer simulations of the model also reveal similar hysteresis behavior in uptake vs chemical potential (pressure) curves at constant temperature (see S.I. Fig. 1,2).

Furthermore, analysis of the model reveals the microscopic origin of hysteresis in this material. In Fig. 3(b) we show the equilibrium isobar of the model (gray), together with a measure of the basic collective timescale of the system (red) and a measure of the curvature of the free-energy surface (blue). The timescale is determined by changing pressure abruptly and measuring the rate of the system’s relaxation to equilibrium (Appendix B). The measure of free-energy curvature, λ , is the smallest eigenvalue of the Hessian matrix of the free energy expressed as a function of occupancies of CO₂ in various binding states (see Appendix C). Near the inflection point of the isobar the system possesses a free-energy landscape that is almost flat, with no strong thermodynamic driving force for CO₂ chains to grow or shrink. As a result, the relaxation time of the system is long, giving rise to hysteresis in the representation of Fig. 2.

In Fig. 4 we show a space-time plot of the model dynamics at the inflection point of the isobar: the microscopic underpinning of the hysteresis seen in Fig. 2 is revealed to be slow diffusive fluctuations of the lengths of polymerized CO₂ chains. By contrast, hysteresis in the presence of a first-order phase transition results from the nucleation of the stable phase in a background of the metastable one.

Conclusions— Cooperative adsorption of gases is of considerable academic and technological importance. Despite recent advances in developing materials in which cooperative adsorption occurs [4–6], we lack complete understanding of how the phenomenon results from the interplay of the molecular constituents of gases and their host framework. This paper puts forth a molecular description of cooperative CO₂ adsorption in the metal-

organic frameworks $\text{Mg}_2(\text{dobpdc})$, using the hysteresis seen in experiment as a means of distinguishing between two possible scenarios. Fundamental understanding of cooperative adsorbers will enable the rational design of these materials; for instance, variation of the energetic binding parameters of the model allows us to set limits on the parameters of the experimental system within which cooperative adsorption occurs, and indicates how to move the inflection point of the isotherm to desired values of temperature and pressure. Fundamental understanding also allows the design of experimental loading protocols that minimize dissipation [34], a first step toward the design of energy-efficient industrial protocols.

ACKNOWLEDGMENTS

The computational portion of this research was carried out as part of a User project at the Molecular Foundry at Lawrence Berkeley National Laboratory (LBNL), supported by the Office of Science, Office of Basic Energy

Sciences, of the U.S. Department of Energy under Contract No. DE-AC02-05CH11231. The experimental portions of the research and the contributions of J.E., R.L.S., Z.P., J.K., and J.R.L. were supported by the Center for Gas Separations, an Energy Frontier Research Center supported by the U.S. Department of Energy, Office of Science, Office of Basic Energy Sciences, under Award DE-SC0001015. J.R.L. serves as a director of and has a financial interest in Mosaic Materials, Inc., a start-up company working to commercialize metal-organic frameworks of the type investigated here. Some of these materials are the subject of patent applications submitted by the University of California, Berkeley. Data availability: All data needed to evaluate the conclusions in the paper are present in the paper and/or the Supplementary Materials. Additional data related to this paper may be requested from the authors. Authors contributions: J.E., J.K., Z.P. and S.W. planned and carried out the simulations, and R.L.S. and J.R.L. did the same for experiments. All authors contributed to the data analysis and interpretation, commented on the results, and drafted the manuscript.

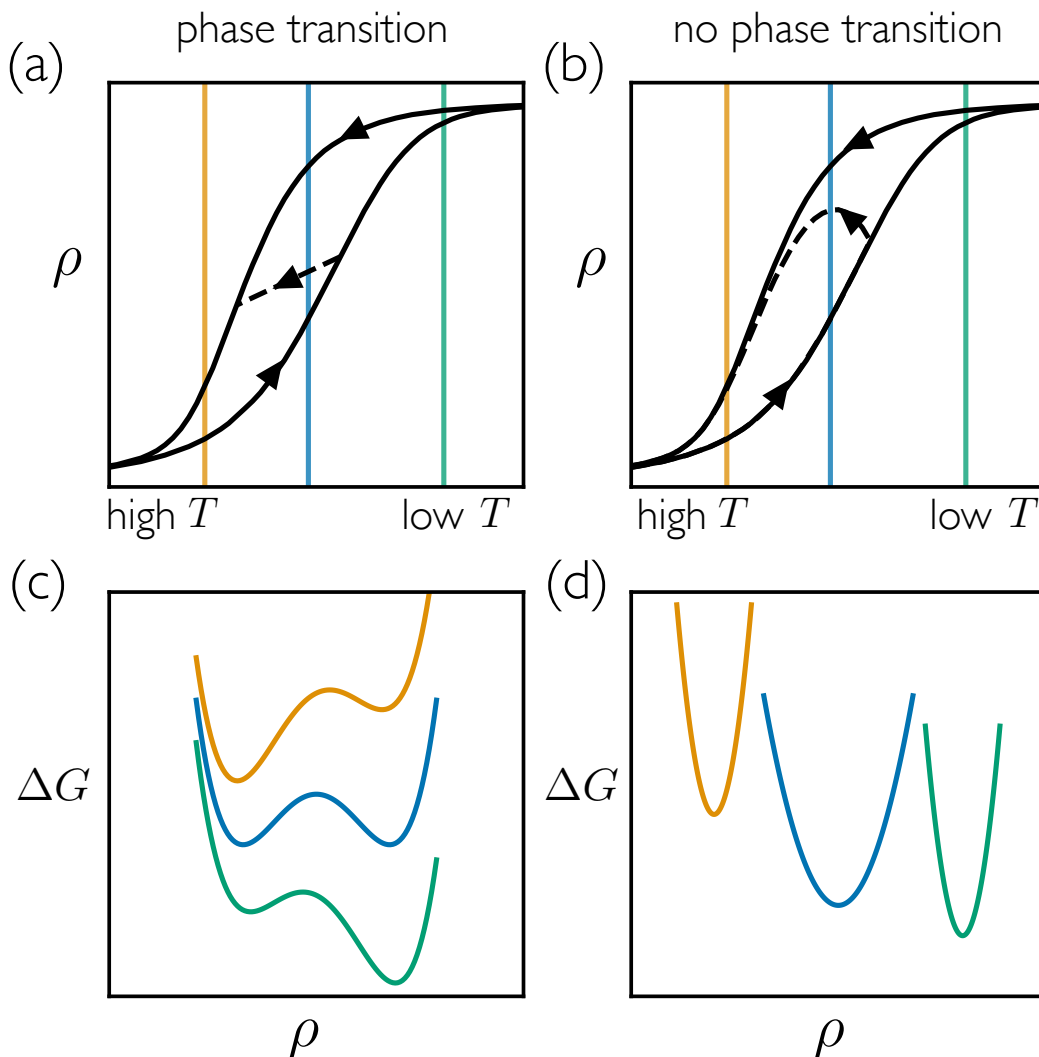


FIG. 1. Schematics of the adsorption-desorption curves along with the corresponding free energy profiles to distinguish between cooperativity with and without an underlying phase transition. (a) Generic adsorption (right) and desorption (left) curves, in an occupancy ρ versus temperature T representation, in the presence of a first-order phase transition. Panel (c) shows associated free-energy (ΔG) profiles. The black dashed line in panel (a) shows an “early stop” desorption scanning curve initiated from partway up the adsorption curve: this desorption curve decreases monotonically as we move left on the figure, because the large timescale required to access the stable state prevents the curve from moving upwards to the point corresponding to the global free-energy minimum. (b) By contrast, desorption curves in the absence of a first-order phase transition are non-monotonic, because the system can evolve toward the global free-energy minimum on the timescale of observation; panel (d) shows associated free-energy profiles. The colored vertical lines in panels (a) and (b) correspond to the similarly-colored profiles in panels (c) and (d), respectively.

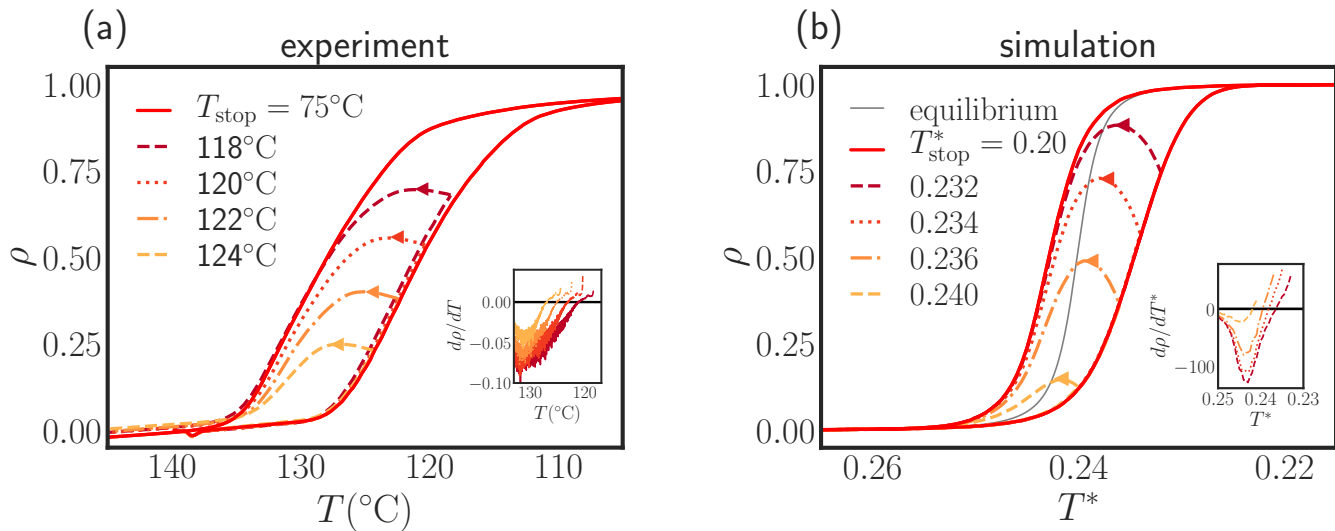


FIG. 2. Scanning curves as obtained in simulations and experiments indicate hysteresis in the absence of a phase transition. Early-stop desorption scanning curves for (a) CO_2 in the MOF e-2- $\text{Mg}_2(\text{dobpdc})$ and (b) our simulation model of the same are consistent with Fig. 1(b): the qualitative nature of hysteresis indicates the *absence* of a phase transition in this MOF. T_{stop} is the temperature at which the scanning curve is reversed. The triangles point in the direction of the scanning curve. The insets to both panels show the gradients of the scanning curves. In panel (b), $T^* \equiv k_{\text{B}}T/\epsilon$, where $\epsilon = 22.6$ kJ/mol is a basic unit of energy. The basic unit of simulation time is determined in Appendix B.

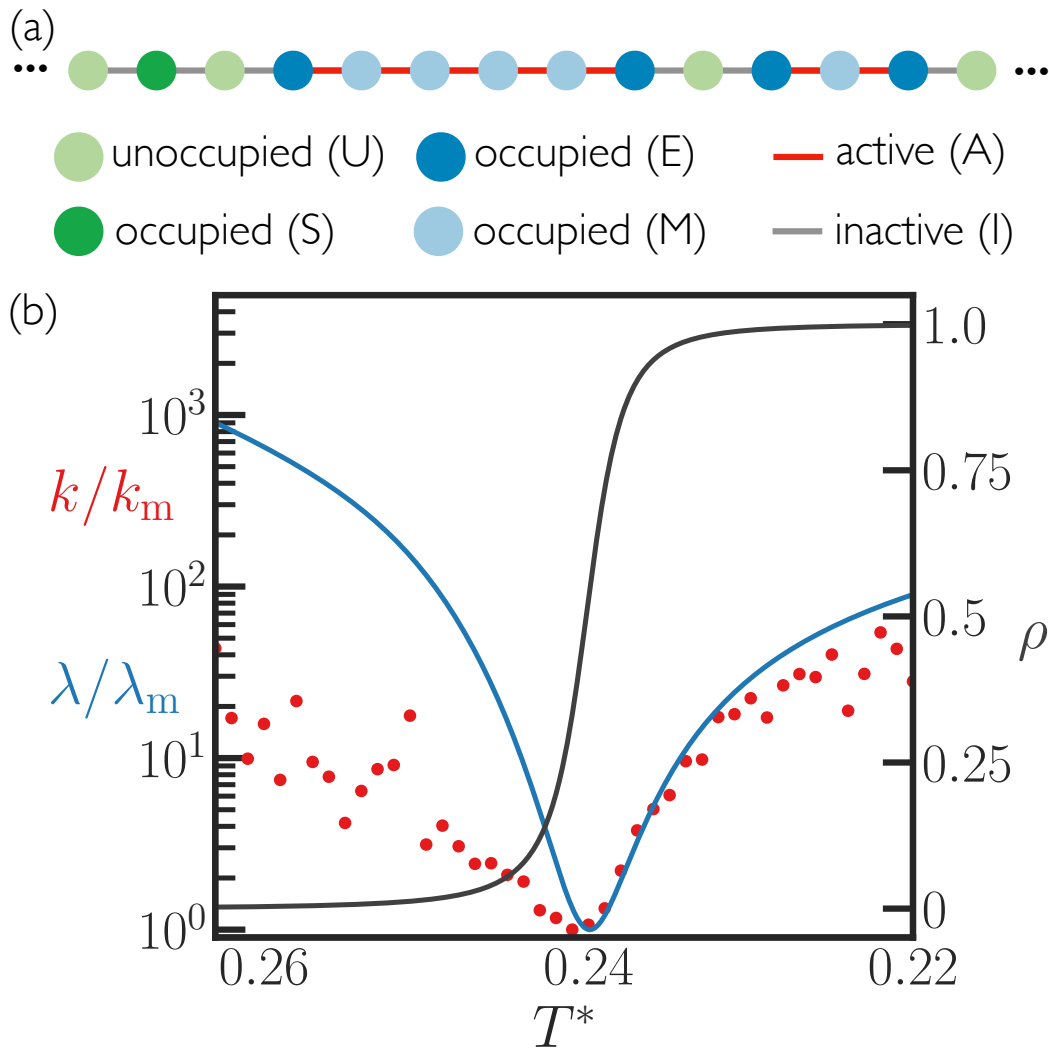


FIG. 3. Statistical mechanical model of the diamine-attached MOF that explains the origin of slow relaxation dynamics near the step position using the flatness of the free energy landscape. (a) Schematic of our statistical mechanical model of a diamine-attached MOF. Each site in the lattice can be unoccupied (U), or occupied by individual CO₂ molecules (S) or molecules at the end (E) or middle (M) of polymerized CO₂ chains. Chains are held together by active (A) bonds; inactive (I) bonds connect all other sites. The rates for changes of these states are given in Appendix B. (b) The approximate curvature of the free-energy landscape of the model, λ , (blue) influences its relaxation rate k (red) along the adsorption isobar (gray). At the inflection point of the isobar the flatness of the free-energy landscape results in slow dynamics and the hysteresis seen in Fig. 2. $k_m \approx 1.30 \times 10^{-9} \text{ s}^{-1}$ and $\lambda_m \approx 0.267$ are reference values of k and λ , respectively (see Appendix B and Appendix C).

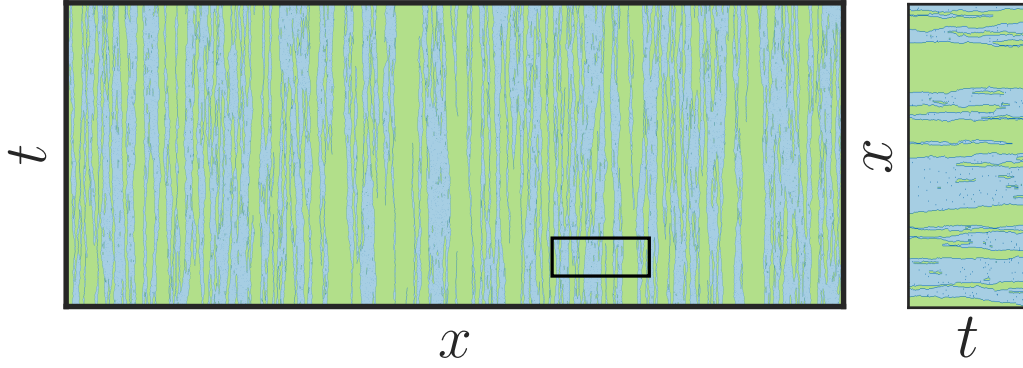


FIG. 4. Large fluctuations in chain length support slow relaxation near the step position. Space x versus time t plot of a trajectory of the lattice model of e-2-Mg₂(dobpdc) at reduced temperature $T^* = 0.24$. Green colors represent unoccupied sites or isolated CO₂ molecules; blue colors represent polymerized CO₂ molecules. The slow dynamics associated with the diffusive fluctuations of chain lengths results in the large relaxation times shown in Fig. 3(b) and the hysteresis shown in Fig. 2(b). The right-hand panel is a zoom of the boxed region.

Appendix A: Experimental Methods

1. General Materials and Methods

All synthetic manipulations were carried out under air. All solvents and the diamine e-2 (*N*-ethylethylenediamine) were purchased from commercial suppliers and used without further purification. The ligand 4,4'-dihydroxy-(1,1'-biphenyl)-3,3'-dicarboxylic acid ($H_4dobpdc$) was obtained from Hangzhou Trylead Chemical Technology Co. Ultra-high purity gases (>99.998%) were used for all adsorption experiments.

2. Synthesis of e-2-Mg₂(dobpdc)

The metal-organic framework Mg₂(dobpdc) was synthesized, washed, and characterized following a previously reported procedure [35]. Post-synthetic functionalization to prepare the diamine-appended framework e-2-Mg₂(dobpdc) was performed as reported previously [35]. The diamine loading was determined following literature procedure [35] by collecting ¹H NMR spectra of material digested with DCl (35 wt % in D₂O) in DMSO-*d*₆. Spectra were collected on a Bruker AMX 300 MHz NMR spectrometer and referenced to residual DMSO (δ 2.50 ppm). The diamine loading of as-synthesized e-2-Mg₂(dobpdc) was found to be 125%, as determined from the ratio of the diamine to ligand peak integrals. A representative diamine loading of 98% was determined following isobar collection. All adsorption data were collected on individual aliquots of a single sample within one week of preparation.

3. Thermogravimetric Analysis

Adsorption and desorption isobars were collected using a TGA Q5000 thermogravimetric analyzer. A flow rate of 10 mL/min was used for all gases, and masses were uncorrected for buoyancy effects. Samples were activated at 120°C for 20 min under pure N₂ before isobar collection. Isobars were measured under pure CO₂ at atmospheric pressure using a temperature ramp rate of 1°C/min.

Appendix B: Simulations

We used the one-dimension version of the model of Ref. [15], sketched in Fig. 3(a), choosing energetic parameters appropriate for the metal Mg. We simulated the model using the Next Reaction Method of Gibson and Bruck [33, 36], whose computation cost per event scales as $\ln N$ for a lattice model of N sites. We allowed the range of processes described in Table I, including the binding and unbinding of CO₂ molecules, and the formation of bonds between them. The stationary distribution of the Markov chain defined by these rates is the grand-canonical probability density of the system.

Event	Rate
U → S	$\omega_0 \exp[\beta(\mu - E_{bs})]$
S → U	$\omega_0 \exp[\beta(E_S - E_{bs})]$
SS[I] → EE[A]	$\omega_0 \exp[-\beta E_{bb}]$
EE[A] → SS[I]	$\omega_0 \exp[\beta(2(E_E - E_S) - E_{bb})]$
EE[I] → MM[A]	$\omega_0 \exp[-\beta E_{bb}]$
MM[A] → EE[I]	$\omega_0 \exp[\beta(2(E_M - E_E) - E_{bb})]$
SE[I] → EM[A]	$\omega_0 \exp[-\beta E_{bb}]$
EM[A] → SE[I]	$\omega_0 \exp[\beta(E_M - E_S - E_{bb})]$
ES[I] → ME[A]	$\omega_0 \exp[-\beta E_{bb}]$
ME[A] → ES[I]	$\omega_0 \exp[\beta(E_M - E_S - E_{bb})]$

TABLE I. List of rates for processes involving single sites (top box) or pairs of neighboring sites and their adjoining bond (bottom box). The energetic parameters are $E_S = -1.0\epsilon$, $E_E = -2.592\epsilon$, $E_M = -3.24\epsilon$, $\beta\mu = -10$, $E_{bs} = 0.5\epsilon$, and $E_{bb} = \epsilon$. Here $\beta = \epsilon/(k_B T)$. The binding energy of a single CO₂ molecule in the MOF ($\epsilon = 22.6$ kJ/mol) is obtained using quantum mechanical density-functional theory [15].

The constants ω_0 and ϵ set the time- and energy scales for the system. The energy scale ϵ is obtained from the binding energy of a single CO₂ molecule on the framework. DFT results from our earlier work Ref. [15] show its value to be $\epsilon = 22.6$ kJ/mol. Following Ref. [15], the binding constants of the gas molecules in the occupied S, M, E states (see Fig. 3(a)) are $E_S = -1.0\epsilon$, $E_E = -2.592\epsilon$ and $E_M = -3.24\epsilon$. We set the activity of the system to be $\beta\mu = -13.5$. We set the barrier height for the site transition to $E_{bs} = 0.5\epsilon$ and the barrier height for all bond transitions to $E_{bb} = \epsilon$, and verified via numerical simulations that small variations in these choices do not affect any of the conclusions of our work. For reasons of computational feasibility we performed the simulations at a higher temperature range than the experiments.

We measured the relaxation rate k in our simulations, displayed in Fig. 3, as follows. The system is initially equilibrated at a certain value of temperature T_0 and activity or pressure P_0 , and has a CO₂ occupancy ρ_0 . We then make an abrupt change in temperature of the of the system. Following this change we measured the CO₂ occupancy $\rho(t)$, averaged over 120 trajectories, until equilibrium is achieved. We compared the final density ρ_f measured in simulations with exact analytical transfer-matrix calculations to ensure that the system has equilibrated. We fit $\bar{\rho}(t) = (\rho_f - \rho(t))/(\rho_f - \rho_0)$ to an exponential form e^{-kt} , thus obtaining k . Values obtained in this way are shown in Fig. 3. We determined the basic time scale of the system, $\omega_0 = 210$ s⁻¹, by equating the relaxation rate measured in experiments (upon an abrupt pressure change) to the relaxation rate of our model k for a step change in pressure at constant temperature.

Appendix C: Analytic treatment of model

As shown in Fig. 3, the curvature of the free energy landscape of our statistical mechanical model is correlated with the slow dynamics of the model. Near the inflection point of the isobar, the free energy landscape is almost flat, implying that the thermodynamic driving force for polymerized CO₂ chains to grow or shrink is small. In this section we detail our calculation of the curvature of the model's free energy.

The grand partition function of the model is given by

$$\mathcal{Z} = \sum_{\{n_1, n_{\text{int}}, n_{\text{end}}\}} K_1^{n_1} K_{\text{end}}^{n_{\text{end}}} K_{\text{int}}^{n_{\text{int}}} \Gamma(n_1, n_{\text{int}}, n_{\text{end}}), \quad (\text{C1})$$

where

$$\Gamma(n_1, n_{\text{int}}, n_{\text{end}}) = \frac{(N - n_{\text{int}} - n_{\text{end}}/2)!}{(N - n_1 - n_{\text{int}} - n_{\text{end}})!(n_{\text{end}}/2)!n_1!} \cdot \frac{(n_{\text{end}}/2 + n_{\text{int}} - 1)!}{(n_{\text{end}}/2 - 1)!n_{\text{int}}!} \quad (\text{C2})$$

is the number of ways of arranging n_1 single molecules, n_{int} internal chain molecules, and n_{end} chain end-points on a one-dimensional lattice of N sites. K_α , with $\alpha \in \{1, \text{int}, \text{end}\}$, is the statistical weight of a CO₂ molecule in conformation α . The free energy in the thermodynamic limit is

$$\begin{aligned} f(x_1, x_{\text{int}}, x_{\text{end}}) = & -(1 - x_{\text{int}} - \frac{x_{\text{end}}}{2}) \ln(1 - x_{\text{int}} - \frac{x_{\text{end}}}{2}) \\ & - (x_{\text{int}} + \frac{x_{\text{end}}}{2}) \ln(x_{\text{int}} + \frac{x_{\text{end}}}{2}) + x_1 \ln x_1 + x_{\text{int}} \ln x_{\text{int}} + x_{\text{end}} \ln \frac{x_{\text{end}}}{2} \\ & + (1 - x_1 - x_{\text{int}} - x_{\text{end}}) \ln(1 - x_1 - x_{\text{int}} - x_{\text{end}}), \end{aligned} \quad (\text{C3})$$

where x_α , with $\alpha \in \{1, \text{int}, \text{end}\}$, is the fraction of CO₂ molecules in conformation α . The Hessian H is a 3×3 matrix built from the three variables x_1 , x_{int} , and x_{end} , with matrix elements

$$H_{\alpha\beta} = \left. \frac{\delta^2 f(x_1, x_{\text{int}}, x_{\text{end}})}{\delta x_\alpha \delta x_\beta} \right|_{\min}, \quad (\text{C4})$$

evaluated at the free-energy minimum.

For a given pressure (the statistical weight K_α is proportional to the pressure), we evaluated $H_{\alpha\beta}$ at the equilibrium values of x_1 , x_{int} , and x_{end} , and calculated the three eigenvalues. We find that the smallest eigenvalue, called λ in Fig. 3(b), becomes very close to zero at the inflection point of the isobar, indicating that there is no strong thermodynamic driving force for the growth or decay of ammonium carbamate chains. As a result, the dynamics of

the model becomes slow, and we show in Fig. 3(b) that the minimum relaxation rate k occurs near the minimum of λ .

-
- [1] D. Britt, H. Furukawa, B. Wang, T. G. Glover, and O. M. Yaghi, “Highly efficient separation of carbon dioxide by a metal-organic framework replete with open metal sites,” *Proc. Natl. Acad. Sci.*, vol. 106, p. 20637, 2009.
- [2] K. Sumida, D. L. Rogow, J. A. Mason, T. M. McDonald, E. D. Bloch, Z. R. Herm, T.-H. Bae, and J. R. Long *Chem. Rev.*, vol. 112, p. 724, 2012.
- [3] H. Furukawa, K. E. Cordova, M. O’Keeffe, and O. M. Yaghi, “The chemistry and applications of metal-organic frameworks,” *Science*, vol. 341, p. 1230444, 2013.
- [4] T. M. McDonald, W. R. Lee, J. A. Mason, B. M. Wiers, C. S. Hong, and J. R. Long, “Capture of carbon dioxide from air and flue gas in the alkylamine-appended metal-organic framework mmen-mg2 (dobpdc),” *J. Am. Chem. Soc.*, vol. 134, p. 7056, 2012.
- [5] T. M. McDonald, J. A. Mason, X. Kong, E. D. Bloch, D. Gygi, A. Dani, V. Crocellà, F. Giordanino, S. O. Odoh, W. S. Drisdell, B. Vlasisavljevich, A. L. Dzubak, R. Poloni, S. K. Schnell, N. Planas, K. Lee, T. Pascal, L. F. Wan, D. Prendergast, J. B. Neaton, B. Smit, J. B. Kortright, L. Gagliardi, S. Bordiga, J. A. Reimer, and J. R. Long *Nature*, vol. 519, p. 303, 2015.
- [6] J. A. Mason, T. M. McDonald, T.-H. Bae, J. E. Bachman, K. Sumida, J. J. Dutton, S. S. Kaye, and J. R. Long *J. Am. Chem. Soc.*, vol. 137, p. 4787, 2015.
- [7] A. Schneemann, V. Bon, I. Schwedler, I. Senkovska, S. Kaskel, and R. A. Fischer *Chem. Soc. Rev.*, vol. 43, p. 6062, 2014.
- [8] E. R. Engel, A. Jouaiti, C. X. Bezuidenhout, M. W. Hosseini, and L. J. Barbour *J. Angew. Chem., Int. Ed.*, vol. 56, p. 8874, 2017.
- [9] F.-X. Coudert, M. Jeffroy, A. H. Fuchs, A. Boutin, and C. Mellot-Drazniéks *J. Am. Chem. Soc.*, vol. 130, p. 14294, 2008.
- [10] C. Triguero, F.-X. Coudert, A. Boutin, A. H. Fuchs, and A. V. Neimark *J. Phys. Chem. Lett.*, vol. 2, p. 2033, 2011.
- [11] D. Bousquet, F.-X. Coudert, A. G. J. Fossati, A. V. Neimark, A. H. Fuchs, and A. Boutin *J. Chem. Phys.*, vol. 138, p. 174706, 2013.
- [12] A. Ghysels, L. Vanduyfhuys, M. Vandichel, M. Waroquier, V. V. Speybroeck, and B. Smit, “On the thermodynamics of framework breathing: A free energy model for gas adsorption in mil-53,” *J. Phys. Chem. C*, vol. 117, p. 11540, 2013.
- [13] C. M. Simon, E. Braun, C. Carraro, and B. Smit, “Statistical mechanical model of gas adsorption in porous crystals with dynamic moieties,” *Proceedings of the National Academy of Sciences*, vol. 114, no. 3, pp. E287–E296, 2017.
- [14] J. J. Binney, N. J. Dowrick, A. J. Fisher, and M. E. Newman, *The theory of critical phenomena: an introduction to the renormalization group*. Oxford University Press, 1992.
- [15] J. Kundu, J. F. Stilck, J.-H. Lee, J. B. Neaton, D. Prendergast, and S. Whitlam, “Cooperative gas adsorption without a phase transition in metal-organic frameworks,” *Physical Review Letters*, vol. 121, p. 015701, 2018.
- [16] R. Evans, “Fluids adsorbed in narrow pores: phase equilibria and structure,” *Journal of Physics: Condensed Matter*, vol. 2, no. 46, p. 8989, 1990.
- [17] P. A. Monson, “Understanding adsorption/desorption hysteresis for fluids in mesoporous materials using simple molecular models and classical density functional theory,” *Microporous and Mesoporous Materials*, vol. 160, pp. 47–66, 2012.
- [18] S. B. Smith, Y. Cui, and C. Bustamante, “Overstretching b-dna: the elastic response of individual double-stranded and single-stranded dna molecules,” *Science*, vol. 271, no. 5250, pp. 795–799, 1996.
- [19] S. Cocco, J. Yan, J.-F. Léger, D. Chatenay, and J. F. Marko, “Overstretching and force-driven strand separation of double-helix dna,” *Physical Review E*, vol. 70, no. 1, p. 011910, 2004.
- [20] S. Whitlam, S. Pronk, and P. L. Geissler, “There and (slowly) back again: entropy-driven hysteresis in a model of dna overstretching,” *BioPhysical journal*, vol. 94, no. 7, pp. 2452–2469, 2008.
- [21] H. Fu, H. Chen, J. F. Marko, and J. Yan, “Two distinct overstretched dna states,” *Nucleic acids research*, vol. 38, no. 16, pp. 5594–5600, 2010.
- [22] Such curves are often referred to as “isobars”, even though the system is not in equilibrium. The true equilibrium isobar has a unique value as a function of temperature.
- [23] D. Wilms, A. Winkler, P. Virnau, and K. Binder, “Rounding of phase transitions in cylindrical pores,” *Physical review letters*, vol. 105, no. 4, p. 045701, 2010.
- [24] P. G. Debenedetti, *Metastable liquids: concepts and principles*. Princeton University Press, 1996.
- [25] D. H. Everett and W. I. Whitton, “A general approach to hysteresis,” *Transactions of the Faraday Society*, vol. 48, pp. 749–757, 1952.
- [26] D. Everett, “A general approach to hysteresis. part 3.—a formal treatment of the independent domain model of hysteresis,” *Transactions of the Faraday Society*, vol. 50, pp. 1077–1096, 1954.
- [27] M. Kruk, M. Jaroniec, and A. Sayari, “Nitrogen adsorption study of mcm-41 molecular sieves synthesized using hydrothermal restructuring,” *Adsorption*, vol. 6, no. 1, pp. 47–51, 2000.
- [28] M. McNall, R. Laurence, and W. C. Conner, “An experimental approach to test sorption mechanisms in mcm-41,” *Microporous and mesoporous materials*, vol. 44, pp. 709–716, 2001.
- [29] G. Tompsett, L. Krogh, D. Griffin, and W. Conner, “Hysteresis and scanning behavior of mesoporous molecular sieves,” *Langmuir*, vol. 21, no. 18, pp. 8214–8225, 2005.

- [30] A. Ghysels, L. Vanduyfhuys, M. Vandichel, M. Waroquier, V. Van Speybroeck, and B. Smit, "On the thermodynamics of framework breathing: A free energy model for gas adsorption in mil-53," *The Journal of Physical Chemistry C*, vol. 117, no. 22, pp. 11540–11554, 2013.
- [31] P. I. Ravikovitch and A. V. Neimark, "Diffusion-controlled hysteresis," *Adsorption*, vol. 11, pp. 265–270, Jul 2005.
- [32] A. C. Forse, M. I. Gonzalez, R. L. Siegelman, V. J. Witherspoon, S. Jawahery, R. Mercado, P. J. Milner, J. D. Martell, B. Smit, B. Blümich, *et al.*, "Unexpected diffusion anisotropy of carbon dioxide in the metal–organic framework zn2 (dobpdc)," *Journal of the American Chemical Society*, vol. 140, no. 5, pp. 1663–1673, 2018.
- [33] M. A. Gibson and J. Bruck, "Efficient exact stochastic simulation of chemical systems with many species and many channels," *The journal of Physical Chemistry A*, vol. 104, no. 9, pp. 1876–1889, 2000.
- [34] U. Seifert, "Entropy production along a stochastic trajectory and an integral fluctuation theorem," *Physical Review Letters*, vol. 95, no. 4, p. 040602, 2005.
- [35] R. L. Siegelman, T. M. McDonald, M. I. Gonzalez, J. D. Martell, P. J. Milner, J. A. Mason, A. H. Berger, A. S. Bhowm, and J. R. Long, "Controlling cooperative co2 adsorption in diamine-appended mg2 (dobpdc) metal–organic frameworks," *Journal of the American Chemical Society*, vol. 139, no. 30, pp. 10526–10538, 2017.
- [36] Y. Li and L. Hu, "A fast exact simulation method for a class of markov jump processes," *The Journal of Chemical Physics*, vol. 143, no. 18, p. 184105, 2015.

Supplemental Information
for
“Hysteresis curves reveal the microscopic origin of cooperative CO₂ adsorption in
diamine-appended metal–organic frameworks”

John R. Edison^{1,2}, Rebecca L. Siegelman^{3,4}, Zdeněk Preisler¹, Joyjit Kundu^{1,5}, Jeffrey R. Long^{3,4,6}, Stephen
Whitelam¹

¹Molecular Foundry, Lawrence Berkeley National Laboratory, 1 Cyclotron Road, Berkeley, CA 94720, USA

²Martin A. Fisher School of Physics, Brandeis University, Waltham, MA 02454, USA

³Department of Chemistry, University of California, Berkeley, CA 94720, USA

⁴Materials Sciences Division, Lawrence Berkeley National Laboratory, Berkeley, CA 94720, USA

⁵Department of Chemistry, Duke University, Durham, NC 27708, USA

⁶Department of Chemical and Biomolecular Engineering, University of California, Berkeley, CA 94720, USA

In figure S2 we show uptake vs chemical potential at constant temperature for the 1D polymerization model. At each value of chemical potential the system evolves for an observation time of 10^8 (reduced units), before we increment or decrement the chemical potential. The dashed line gives the exact equilibrium density and is computed using Transfer Matrix calculations. The behavior of the scanning curves is qualitatively similar to the case where we compute uptake vs temperature at fixed pressure. Below we show snapshots from a long-time simulation run at three different values of chemical potential i) Low ($\beta\mu = 29.14$) ii) Near the transition ($\beta\mu = -28.57$) iii) High ($\beta\mu = -28.0$).

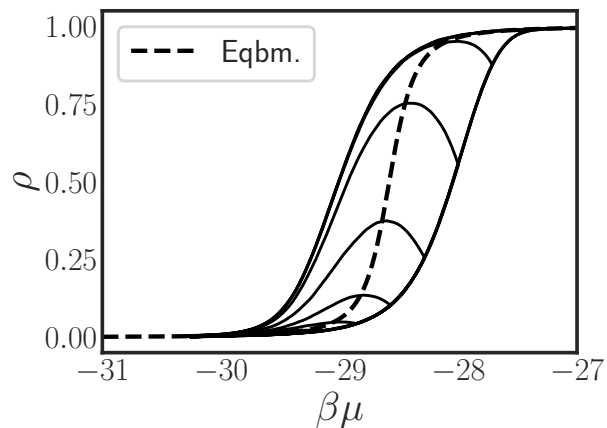


FIG. S1. Typical equilibrium uptake, hysteresis curve and an early-stop desorption scanning curves for a given set of parameters. Simulated uptake curves as a function of chemical potential $\beta\mu$ at constant temperature are qualitatively similar to the uptake curves as a function of temperature reported in the main text [parameters: $E_s = 1.0$, $E_m = 2.5$, $E_t = 2.0$ and $T^* = 0.175$]. The observation time in reduced units in 10^8 .

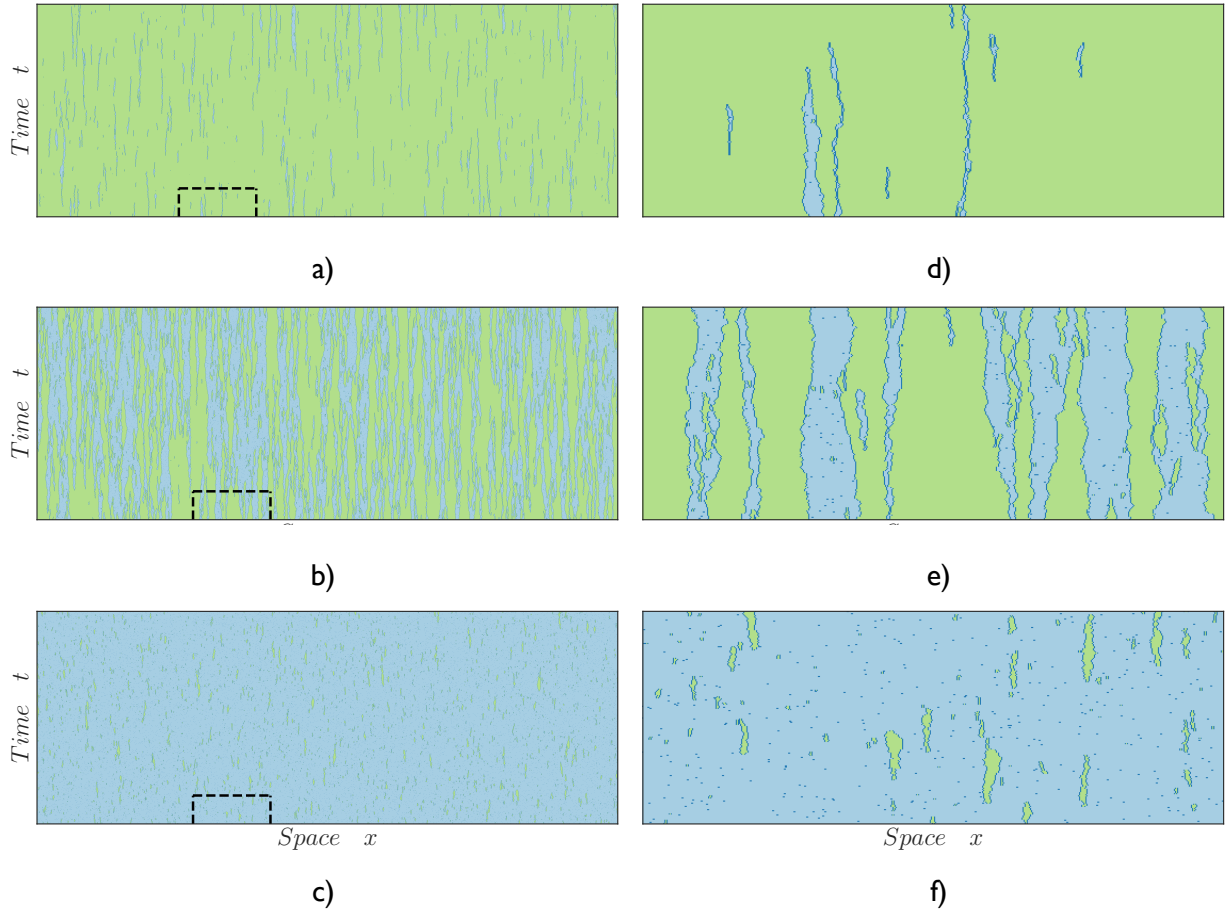


FIG. S2. Figs a-c) are plots of time evolutions of the model where we study the evolution of the system for a step-change in chemical potential at fixed temperature. The run times of these simulations are much larger than the respective relaxation times. The values of chemical potential for the plots are a) $\beta\mu = 29.14$) b) $\beta\mu = -28.57$) and c) $\beta\mu = -28.0$. The region within the dashed-box area in plots a-c) are shown in plots d-f). Green colors represent unoccupied sites or isolated CO₂ molecules; blue colors represent polymerized CO₂ molecules.